JOURNAL OF GEOPHYSICAL RESEARCH, VOL. 110, D08205, doi:10.1029/2004JD005350, 2005

Correction published 28 June 2005

Pyro-cumulonimbus injection of smoke to the stratosphere: Observations and impact of a super blowup in northwestern Canada on 3–4 August 1998

Michael Fromm,[1] Richard Bevilacqua,[1] René Servranckx,[2] James Rosen,[3] Jeffrey P. Thayer,[4] Jay Herman,[5] and David Larko[6]

Received 13 August 2004; revised 2 November 2004; accepted 11 February 2005; published 30 April 2005.

[1] We report observations and analysis of a pyro-cumulonimbus event in the midst of a boreal forest fire blowup in Northwest Territories Canada, near Norman Wells, on 3–4 August 1998. We find that this blowup caused a five-fold increase in lower stratospheric aerosol burden, as well as multiple reports of anomalous enhancements of tropospheric gases and aerosols across Europe 1 week later. Our observations come from solar occultation satellites (POAM III and SAGE II), nadir imagers (GOES, AVHRR, SeaWiFS, DMSP), TOMS, lidar, and backscattersonde. First, we provide a detailed analysis of the 3 August eruption of extreme pyro-convection. This includes identifying the specific pyro-cumulonimbus cells that caused the lower stratospheric aerosol injection, and a meteorological analysis. Next, we characterize the altitude, composition, and opacity of the post-convection smoke plume on 4–7 August. Finally, the stratospheric impact of this injection is analyzed. Satellite images reveal two noteworthy pyro-cumulonimbus phenomena: (1) an active-convection cloud top containing enough smoke to visibly alter the reflectivity of the cloud anvil in the Upper Troposphere Lower Stratosphere (UTLS) and (2) a smoke plume, that endured for at least 2 hours, atop an anvil. The smoke pall deposited by the Norman Wells pyro-convection was a very large, optically dense, UTLS-level plume on 4 August that exhibited a mesoscale cyclonic circulation. An analysis of plume color/texture from SeaWiFS data, aerosol index, and brightness temperature establishes the extreme altitude and ''pure'' smoke composition of this unique plume. We show what we believe to be a first-ever measurement of strongly enhanced ozone in the lower stratosphere mingled with smoke layers. We conclude that two to four extreme pyro-thunderstorms near Norman Wells created a smoke injection of hemispheric scope that substantially increased stratospheric optical depth, transported aerosols 7 km above the tropopause (above ~430 K potential temperature), and also perturbed lower stratospheric ozone.

Citation: Fromm, M., R. Bevilacqua, R. Servranckx, J. Rosen, J. P. Thayer, J. Herman, and D. Larko (2005), Pyro-cumulonimbus injection of smoke to the stratosphere: Observations and impact of a super blowup in northwestern Canada on 3–4 August 1998, *J. Geophys. Res.*, *110*, D08205, doi:10.1029/2004JD005350.

1. Introduction

[2] There is growing evidence that a newly discovered force for explosive troposphere-to-stratosphere transport (TST), a dynamic combination of extreme boreal forest fire and convection (which we will refer to herein as ''pyro-cumulonimbus'' or ''pyroCb'') [*Fromm and Servranckx*, 2003] (hereinafter referred to as FS03), operates repeatedly and may have an important regional or hemispheric atmospheric impact. The northern summer of 1998 was punctuated by multiple pyroCb blowups, one episode (in Canada in early July) being described in detail by *Fromm et al.* [2000]. A second event, originating in Canada on 3 and 4 August, but until now not well characterized, was shown to be responsible for noteworthy long-distance transport of tropospheric aerosols [*Hsu et al.*, 1999a; *Forster et al.*, 2001; *O'Neill et al.*, 2002; *Fiebig et al.*, 2002; *Formenti et al.*, 2002; *Wandinger et al.*, 2002], carbon monoxide [*Forster et al.*, 2001], and NO_X [*Spichtinger et al.*, 2001]

[1]Naval Research Laboratory, Washington, D. C., USA.
[2]Canadian Meteorological Centre, Dorval, Quebec, Canada.
[3]Department of Physics and Astronomy, University of Wyoming, Laramie, Wyoming, USA.
[4]Department of Aerospace Engineering Sciences, University of Colorado, Boulder, Colorado, USA.
[5]NASA Goddard Space Flight Center, Greenbelt, Maryland, USA.
[6]Science Systems and Applications, Inc., Lanham, Maryland, USA.

0148-0227/05/2004JD005350$09.00

to western Europe. Soon after this early August fire blowup, lower stratospheric aerosol optical depth rapidly increased by a factor of 5 over early summer values [*Fromm et al.*, 2000].

[3] In addition to the remarkable events of 1998, there have been other discoveries of pyroCb-related TST. The investigation of FS03, which linked a specific pyroCb (the Chisholm fire in Alberta Canada) to TST in the boreal spring of 2001, was motivated by numerous satellite and lidar observations of stratospheric aerosol layers similar to those of 1998. An August 1992 pyroCb blowup was shown to be the cause for stratospheric enhancements of methyl cyanide [*Livesey et al.*, 2004]. In the summer of 2002, during NASA's Cirrus Regional Study of Tropical Anvils and Cirrus Layers Florida Area Cirrus Experiment (CRYSTAL-FACE) mission, remote and in situ observations of stratospheric enhancements of peculiarly biomass-related gaseous and particulate species were traced back to fires in Canada in late June [*Jost et al.*, 2004]. This type of TST may have occurred as well in September 1950, when a persistent fire in Alberta [*Murphy and Tymstra*, 1986] developed into a firestorm responsible for creating a historic smoke pall that caused observations of blue suns and moons in the United States and Europe. This particular smoke plume was observed visually by aircraft pilots, scrambled expressly for plume identification, over Scotland at an altitude of 13 km [*Penndorf*, 1953].

[4] Convection in thunderstorms is sufficiently energetic in some circumstances to transfer material from the lower troposphere into the upper troposphere and lower stratosphere (UTLS) [e.g., *Poulida et al.*, 1996]. However, it is generally accepted that only volcanic eruptions have the energy to cause deep stratospheric injection of surface and tropospheric boundary layer material. In a recent modeling study of midlatitude supercell thunderstorms, *Wang* [2003] reproduced a tropopause-level plume feature observed above thunderstorm anvil cloud tops by satellites and showed that these plumes can signify significant transport of tropospheric water vapor into the lowermost stratosphere. This suggests that extreme convection, even unassociated with energetic forest fires, may represent an important pathway for rapid, efficient redistribution of critical gases and particles from the lowest levels of the atmosphere to the lower stratosphere (LS). Combined with biomass burning, which is increasingly acknowledged to be an important but poorly characterized factor in atmospheric and climate processes [e.g., *Lindesay et al.*, 1996; *Kasischke and Penner*, 2004], extreme pyro-convection may now represent an important, recurring mechanism contributing to troposphere to stratosphere exchange. A recurring pyro-convective transport mechanism may represent a separate pathway for stratosphere-troposphere exchange to be considered along with the better understood, "traditional" means [e.g., *Stohl et al.*, 2003; *Holton et al.*, 1995]. Because pyro-convection is naturally associated with abundant pollutants such as CO, NOx, and smoke, the potential for significant atmospheric impact is potentially much greater than for "regular" convection.

[5] We have two aims for this paper: (1) to present observational details of a "smoking gun" pyroCb event on 3–4 August 1998 (hereinafter referred to as the Norman Wells pyroCb, after the town in Canada's Northwest Territories (NWT) closest to the blowup); this smoking gun was the source of material transported to Europe, detailed by the above-mentioned investigators, as well as the five-fold increase in POAM III stratospheric aerosol optical depth; and (2) to characterize the downstream stratospheric impact of this remarkable TST event. The discussion of the downstream impact will show for the first time an enhancement of lower stratospheric ozone related to biomass-burning plume injection.

[6] In section 2 we present our analysis of the satellite observations of the pyroCb and residual UTLS smoke plume. Section 2 also contains the meteorological analysis of the blowup environment. Section 3 is an analysis of the stratospheric impact of this TST event, focusing on the month of August 1998. Conclusions and final discussion are contained in section 4.

2. The 3–4 August Norman Wells PyroCb

[7] As mentioned in section 1 the pyro-convective events of 3–4 August in Northwest Territories had a great impact on both the troposphere and stratosphere. As we will develop in this section, the convective activity included multiple cells, of varying intensity and duration. We focus our analysis of convection in this section to two pyroCbs, one that reveals much about unique pyroCb cloud microphysics, and the other being the main source for the stratospheric injection of smoke.

2.1. Satellite Analysis of the Blowup

[8] Fire activity in Canada in 1998, monitored by satellite-detected hot spot count, increased in July, and reached a sharp peak in early August [*Fromm et al.*, 2000]. On 3 August, many of the hot spots were concentrated in the Yukon and NWT. Figure 1 is a view from AVHRR of a portion of NWT near Great Bear Lake and Norman Wells (65.3°N, 126.8°W), on 3 August at 0117 UTC (local time is UTC minus 7 hours; thus this is late afternoon). Figure 1a is a false-color rendering (red-channel 3, 3.7 μm; green-channel 2, 0.9 μm; and blue-channel 1, 0.6 μm). Here the fire hot spots are distinctively red. The abundance of fires and smoke plumes is evident. The clouds in this scene are predominantly cirrus and scattered small cumulus. The 10.7 μm IR brightness temperature (T_b), shown in Figure 1b, does not indicate any deep convective clouds at this time in the area of the fires west of Great Bear Lake. (Here and elsewhere we use the well-known method of inferring cloud top height by invoking IR T_b, sometimes in relation to nearby radiosonde profiles. A good review of the method and its limitations is presented by *Sherwood et al.* [2004]).

[9] Roughly 24 hours later, at 0055 UTC on 4 August (Figure 2) the scene contained a wider variety of action. The several hot spots were still evident. Some of the hot spots were producing only low, fanning smoke plumes while others were associated with convective cloud/plume development. Convection stages in this scene varied from nascent to mature; some cells were connected to hot spots, and some were not. The IR view (Figure 2b) reveals that some of the convective cells had cold (i.e., deep) cloud

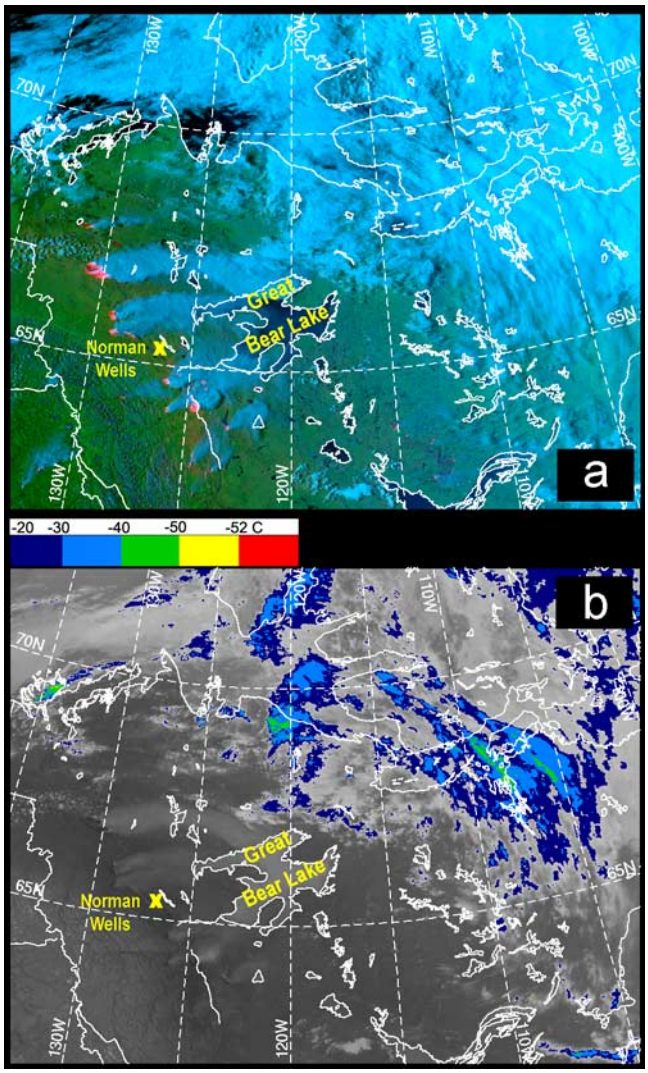

Figure 1. AVHRR image, 3 August, 0117 UTC, northwestern Canada. Norman Wells is located at the yellow cross. Lake in center of image is Great Bear Lake. (a) RGB image (see text for details). (b) IR (10.7 μm) brightness temperature (°C). Note that all AVHRR and GOES image projections are polar stereographic.

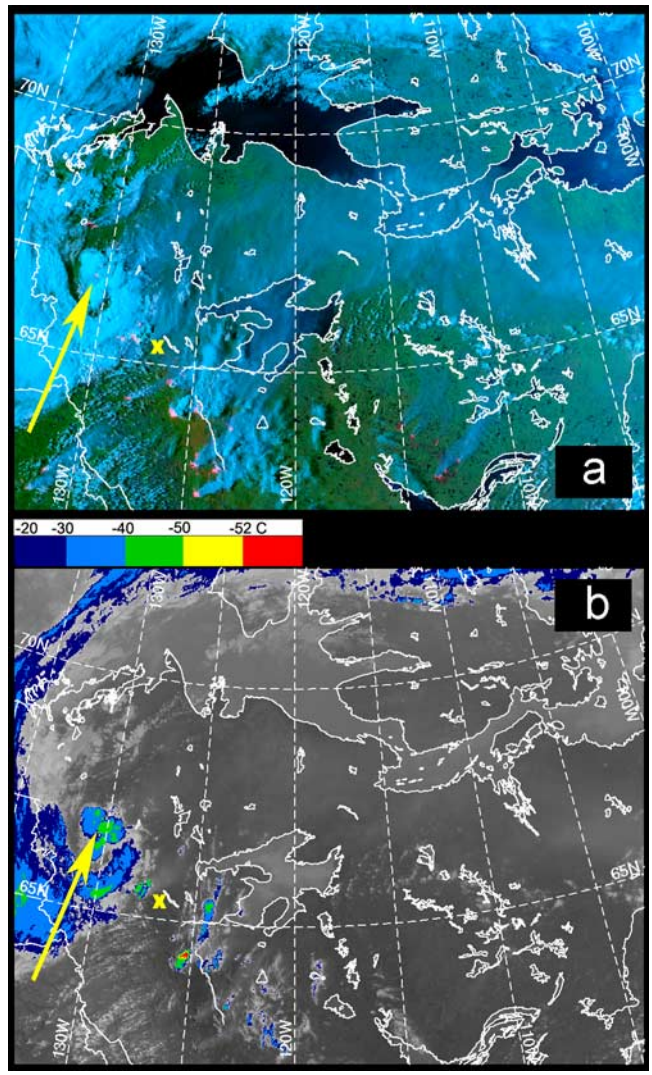

Figure 2. AVHRR image, 4 August 1998, 0055 UTC. Domain is same as Figure 1. (a) RGB. (b) IR. Arrow shows convective cluster focused on in Figure 4.

tops. The coldest of these had brightness temperatures (T_b) between −50° and −55°C, which placed these cloud tops in the vicinity of, and perhaps even above, the tropopause, based on the Norman Wells radiosonde measurements at 0000 UTC, 4 August (Figure 3). We see in Figure 3 that the radiosonde temperature is greater than −50°C from an altitude of approximately 16 km downward. The tropopause is at 9 km. Thus the minimum T_b values may place some of these cloud tops as much as 7 km above the tropopause.

[10] The AVHRR imagery at 0055 UTC captures a set of signatures revealing that pyro-convection is dramatically unique. For instance, the arrow in Figure 2 points to a convective cloud cluster. We focus on that cluster in Figure 4. Figure 4a is a conventional black/white rendering of the visible (AVHRR channel 1, 0.6 μm) reflectance, and Figure 4b is the near-IR 3.7 μm T_b (Figure 4b) qualitatively

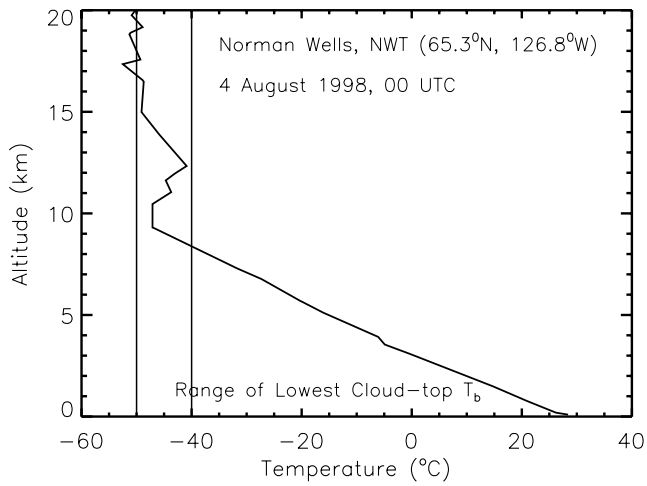

Figure 3. Norman Wells radiosonde temperature profile, 0000 UTC, 4 August 1998.

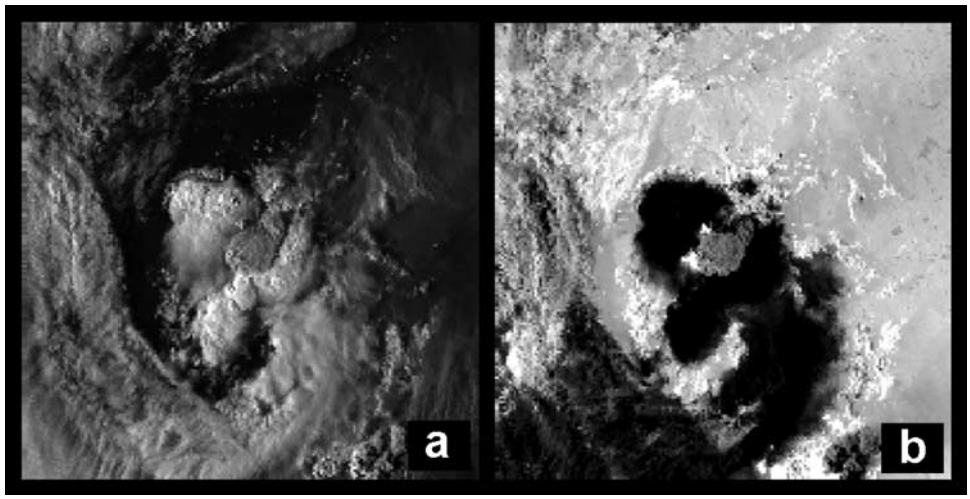

Figure 4. Close-up AVHRR view of convective cluster at 0055 UTC, 4 August 1998, northwest of Norman Wells. (a) Gray scale image of visible-channel (0.63 μm) with highest reflectivity as white. (b) Gray scale image of 3.7 μm radiance. Low radiance, black; high radiance, white. AVHRR-measured radiance at 3.7 μm in sunlit conditions is a combination of emitted IR and reflected visible radiation.

rendered in a gray scale that goes from black/cold to white/warm. In the visible image (Figure 4a), the top of the anvil cloud in the middle of the cluster (and in the center of the figure panel) has a perceptibly grayer appearance than its neighbors. Figure 4b shows two hot spots (the very bright white features along the western and northern flank of the anvil) associated with this cloud; thus it is likely a pyroCb. (In addition to this pyroCb, there is yet another in an active phase of development, seen along the bottom right of Figure 4 and in Figure 2a, just northwest of the Norman Wells symbol. This convection will be referred to in the discussion of Figures 5 and 6.) In addition to being grayish at visible wavelengths (Figure 4a), the anvil is as cold or even colder than its neighbors. (See the IR image in Figure 2b. The entire anvil is shaded green versus patchy blue/green in the neighboring clouds.) Thus it is likely deeper than its neighbors and at temperatures $<-40°C$, below the threshold for homogeneous nucleation of ice [*Wallace and Hobbs*, 1977]. The 3.7 μm T_b (Figure 4b) further distinguishes this cloud; it is uniformly higher (i.e., it is brighter) than that of the surrounding clouds. In this sunlit view, which from the standpoint of the 3.7 μm radiance is

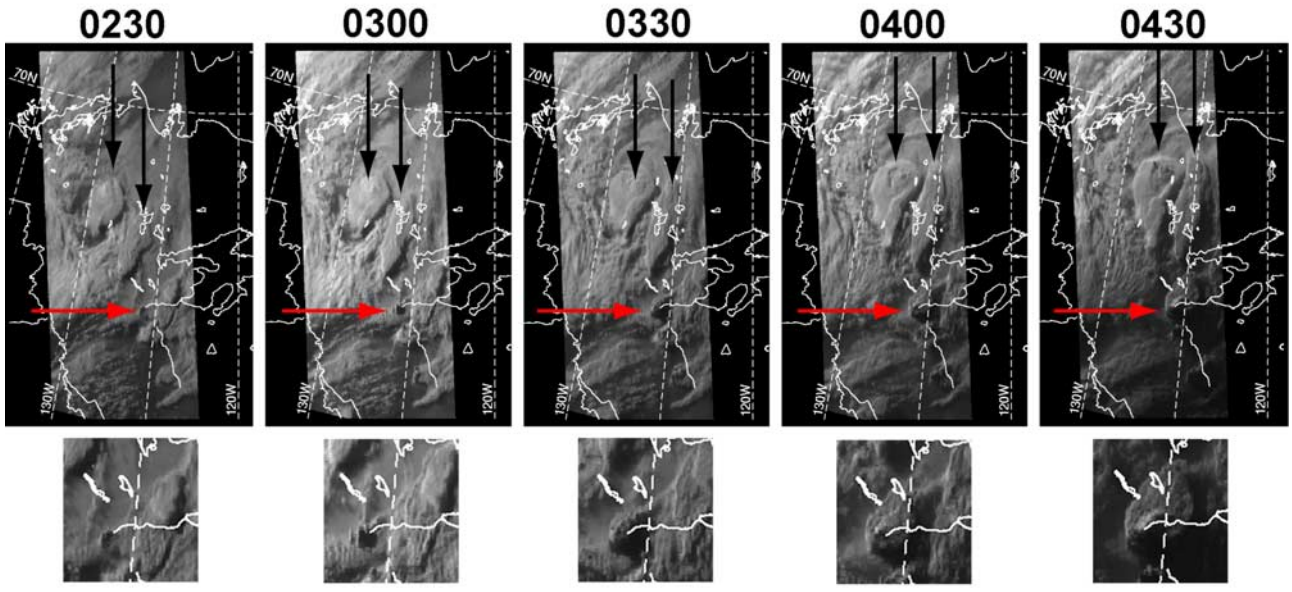

Figure 5. (top) Gray scale GOES West visible-channel (0.62 μm) image sequence, northwestern Canada, 4 August 1998, 0230–0430 UTC. Black arrows point to two clouds that originated northwest of Norman Wells, and are discussed in relation to Figure 4. Red arrows point to Norman Wells pyroCb in development. (bottom) zoomed images of Norman Wells pyroCb.

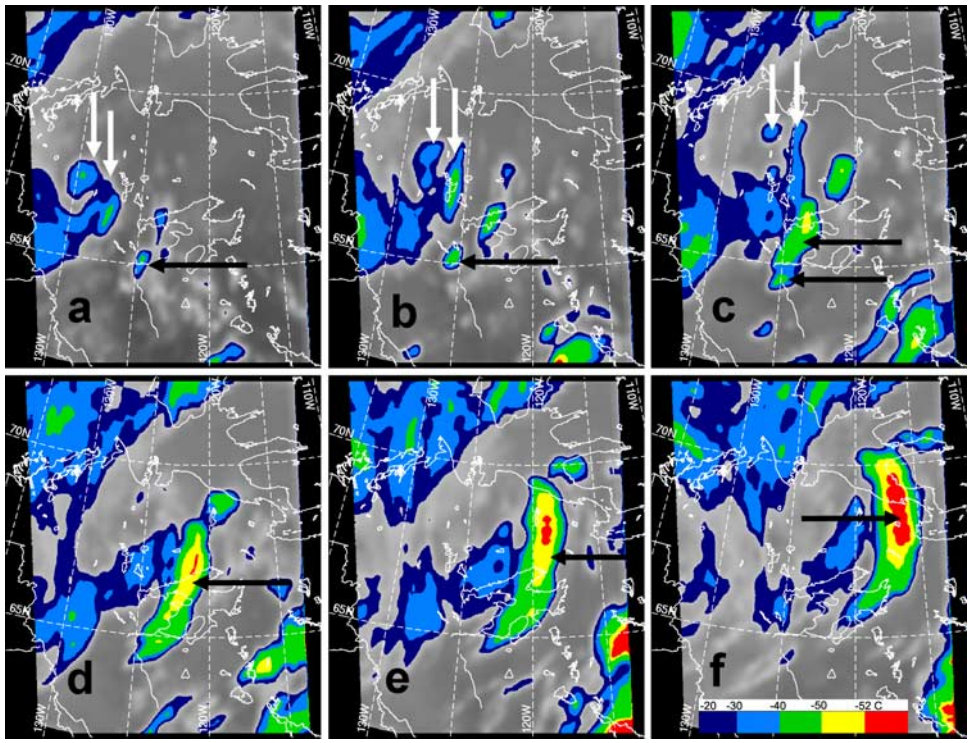

Figure 6. GOES IR 10.7 μm brightness temperature, 4 August 1998, northwestern Canada. Left to right: (top) 0200, 0400, and 0600 UTC; (bottom) 0800, 1000, and 1200 UTC. Color-coded temperature scale is same as for AVHRR IR imagery.

impacted both by emitted and reflected radiation [*Arking and Childs*, 1985], the "warm" 3.7 μm T_b indicates a population of cloud particles distinctly smaller than that of the presumably glaciated cloud top ice crystals in the surrounding anvils. Thus it appears that in this pyro-convective cell, smoke particles rose to the cloud top level in sufficient number to measurably reduce the visible reflectance and enhance near-IR reflectance of the cloud. In short, it appears that the very deep pyroCb cloud top is polluted with smoke and/or smoke-encrusted water-ice crystals, perhaps an extreme manifestation of the phenomenon reported by *Andreae et al.* [2004].

[11] It is certainly fortunate that the intensification of some fires and convection in this case occurred during daylight, for it helped to illustrate the unique character of deep pyro-convection and its cloud impact. Sunlight on the convective cloud tops discussed above enabled us to differentiate the characteristics of a UTLS-level pyroCb anvil cloud from "normal" convection: visibly gray and uniformly warmer at 3.7 μm (in addition to being deeper than other anvils). However, that particular cell, as peculiar as it was, was in our view not the primary pathway for the UTLS smoke plume that is the subject of this paper. For that we shift our attention approximately 200 km to the southeast, where the deepest smoke "eruption" occurred and persisted after sunset. In Figure 2b this pyro-convection stands out for its deeper/colder cloud top (red shading).

[12] In the hours after the 0055 UTC imagery, convective events started or continued over several additional hot spots and also in locations with no apparent fire activity. Figure 5 is a Geostationary Operational Environmental Satellite (GOES) West visible image sequence of this region between 0230 and 0430 UTC. At this time the clouds associated with the convection discussed in relation to Figure 4 evolved into a pair of large, broad and deep shrouds, north of Norman Wells (black arrows in Figure 5). Roughly 70 km southeast of Norman Wells, near hot spots and convection that were also evident in Figure 2, is another active convective cell, identified by the red arrow in Figure 5, and zoomed in on in the lower portion of Figure 5. The low zenith angle illumination gives stark details, even at the relatively poor GOES resolution of 16 km at these high latitudes. At 0230 UTC the young cell is a small yet identifiable feature illuminated toward the northwest and shadowed toward the southeast. At 0300 UTC a lengthening shadow indicates growing convection. At 0330 UTC, violent development is apparent. The cell's cloud top has spread substantially, and there is a strong hint of a turret protruding above the broad cloud top. This plume above the anvil becomes more striking at 0400 UTC. Here again we point to illumination on the sun-facing side, and shadowing opposite, which exposes a V-shaped structure spreading northeast from the south-center of the anvil. This plume feature persists and becomes even easier to identify at 0430 UTC. We used the horizontal length (parallel to the solar azimuth direction) of the illuminated side of the turret, in conjunction with solar elevation angle at this time and place (3.8°), to estimate its height. Calculating the rise from several points gave elevation roughly 1±0.5 km. We also examined visible imagery from the Defense Meteorological Satellite Program (DMSP) Operational Line Scan (OLS) (http://dmsp.ngdc.noaa.gov/html/sensors/doc_ols.html) to study this pyroCb. An image

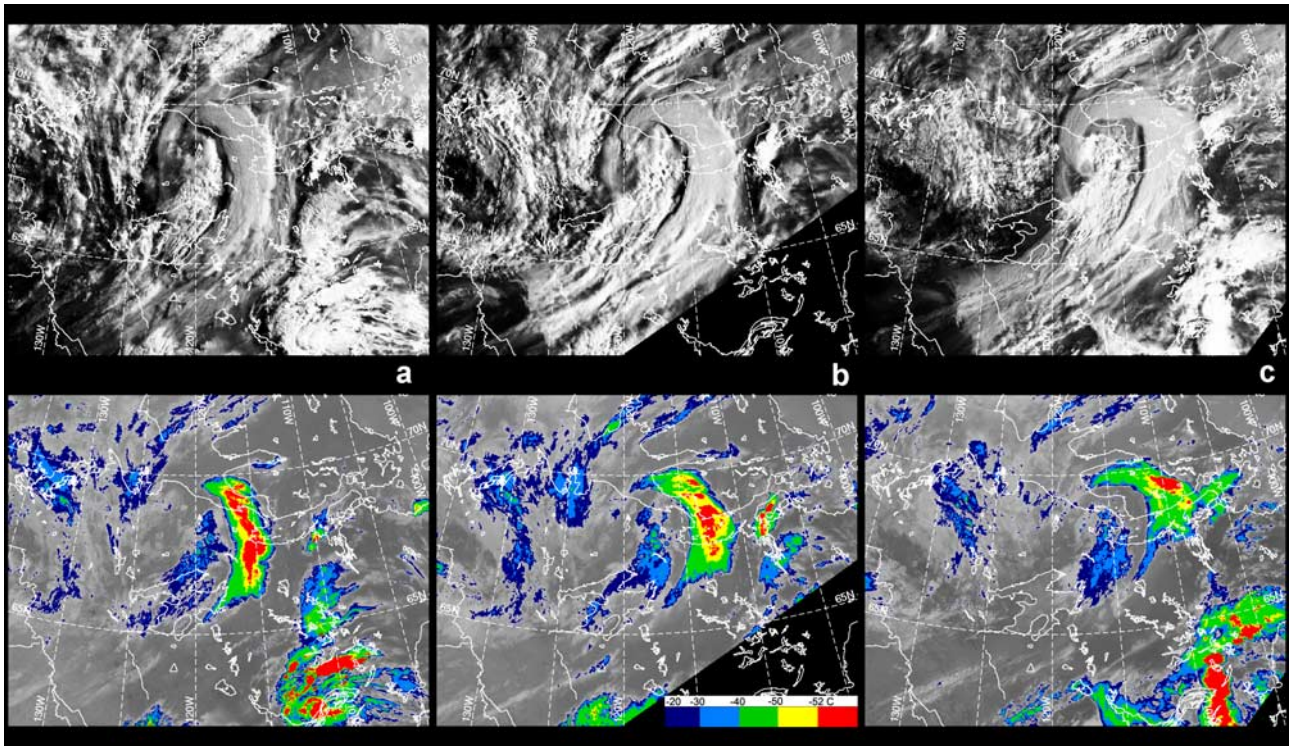

Figure 7. AVHRR visible and IR images at (a) 1241, (b) 1422, and (c) 1618 UTC, 4 August 1998, northwestern Canada. Domain is same as in Figures 1 and 2.

at 0518 UTC (not shown) also captures the expansive plume atop the anvil. Thus this convection appears to have been sufficiently energetic to generate a plume that endured for at least 2 hours. It is not possible to determine the composition of the plume material, but based on the analysis of the earlier pyroCb (Figure 4), we conjecture that it included a considerable amount of smoke. We believe this Norman Wells pyroCb was primarily responsible for the UTLS smoke transport that is the focus of this study.

[13] Because the activity persisted after sunset, we follow it with GOES IR (10.7 μm) imagery (Figure 6). In the interval between 0200 and 1200 UTC it is apparent that multiple cells grew and reached high altitude. This sequence shows that the pyroCbs northwest of Norman Wells (discussed in relation to Figure 4) produced an opaque and fairly deep, persistent cloud (white arrows). However, the sequence of images is dominated by one feature (black arrow), an enormous shroud of cold/deep material that spread north-northeast, and which was still evident at 1200 UTC, long after the convection had collapsed. The genesis of this cloud was at about 0100 UTC, the point source being the plume-bearing Norman Wells pyroCb. Close inspection of the GOES IR and visible-channel sequence at half-hourly intervals reveals that three to four pyroCbs exploded in close proximity between roughly 0200 and 0500 UTC. It is evident from the sequence in Figure 6 that between storm genesis and 0800 to 1000 UTC, the cloud remained anchored to the point near the hot spots, indicating that the firestorm persisted on the order of 8 hours. Even at 1200 UTC, a few hours after the huge shroud moved away from the source hot spots, there is another small cloud feature at the hot spot site, indicating perhaps yet another pyro-convective cell. The T_b on much of the huge shroud was below −52°C, which is significantly lower than the Norman Wells 0000 UTC tropopause temperature (−47°C). The area enclosed by the −52°C contour increased through most of the night, possibly suggesting that the top of the cloud deepened. Thus the shroud spawned by the Norman Wells pyroCbs persisted, expanded, and exhibited low temperatures characteristic of the lowermost stratosphere throughout the night. Moreover, it is evident that in our NWT focus area, there was an expansive range of pyro-convective intensity on 3–4 August that resulted in transport of smoke (and thus other emissions) throughout the free troposphere and into the lowermost stratosphere.

2.2. Analysis of the Post-Convection Plume

[14] After sunrise on 4 August, a 4-hour sequence of visible and IR imagery from AVHRR (Figure 7) details a stunning and unique cloud form northeast of our focus area of the night before. It is expansive, distinctly gray throughout, and very cold over a substantial portion of this croissant-shaped feature. It has evolved from the 1200 UTC GOES view but is obviously the same cloud feature. That is, this "croissant" cloud traces its origin back to the Norman Wells pyroCb. The coldest T_b at this time was still close to the tropopause temperature. The croissant cloud has the same distinctive and highly unusual pair of qualities, gray (especially as compared to bright white mature convective cells to the south) in the visible and very cold in the IR, as the Chisholm smoke plume described by FS03. A close examination of the visible image in Figure 7c at 1618 UTC gives the impression that the texture of the

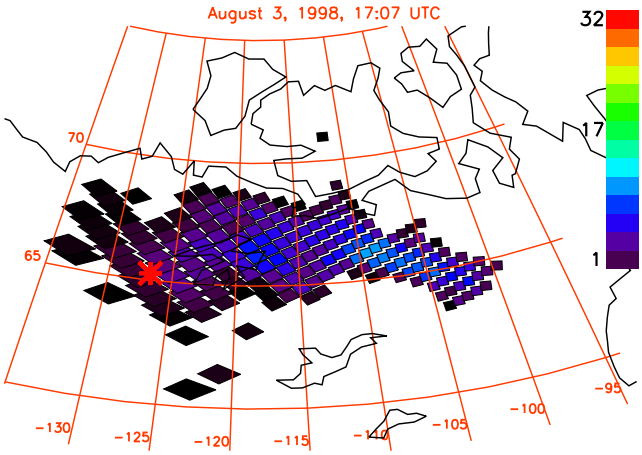

Figure 8. TOMS version 8 aerosol index (AI) map, 3 August 1998, northwestern Canada. Projection is polar stereographic; domain is approximately the same as AVHRR images in Figures 1, 2, and 7. Norman Wells location is shown by the red asterisk. Single orbit of TOMS level 2 AI is shown, mapped onto TOMS field-of-view "footprint." Measurement time is roughly 1707 UTC. AI values below 1.0 are not shown. Rainbow color scale range used for AI is fixed, between AI = 1 and AI = 32, for this and Figures 9 and 10.

croissant cloud is unlike any of the water-ice clouds in this scene. In the northeast quadrant of the cloud, there is no apparent variability in the cloud top surface; it is almost totally smooth. In other parts of the croissant cloud (e.g., in the northwest segment), there is a striated texture that is also different than any of the water-ice cloud forms. Although not shown, the AVHRR 3.7 μm radiance of the croissant cloud was uniformly greater than that of neighboring deep water-ice cloud tops, implying it has the same small-particle population in comparison with the other deep clouds as seen in Figure 4b. These early morning views give the first hints that the cloud/plume that came from the Norman Wells pyroCb was dominated by a peculiar, smokey composition. The three-image sequence between 1241 and 1618 UTC also plainly shows a developing cyclonic circulation in the croissant cloud, which will be discussed further later in this section. On the basis of these interpretations and those that follow, we hold that the Norman Wells pyroCb was the "smoking gun" event that produced the deep, opaque, peculiar croissant cloud, and afterward the preponderance of the POAM/SAGE-observed stratospheric aerosol increase in the boreal summer and autumn of 1998 shown by *Fromm et al.* [2000].

2.2.1. Plume Composition and Depth

[15] We use the Total Ozone Mapping Spectrometer (TOMS) level-two aerosol index (AI), as did FS03, to verify the composition of the croissant-shaped cloud and compare it with the pre-blowup smoke plume of 3 August. To first order, positive TOMS AI is increased by increasing aerosol optical depth, reducing single scatter albedo, or increasing aerosol-layer altitude. We analyze AI here strictly for conditions where the single scatter albedo is essentially invariable (i.e., the smoke aerosols have a common origin). Hence variations in AI are probably limited to variations in plume height and optical depth. Here we use the version 8 TOMS product, which offers distinct advantages over version 7 used by FS03. For instance, version 8 AI is unencumbered by the artificial maximum value of 12.8 in version 7. Here the values reflect the full range of aerosol index intensities revealed by extreme events such as this. This is important, since the AI increases rapidly with altitude for the same amount of aerosol present in the atmosphere, and the values of AI are enhanced when smoke is present over a bright surface such as a cloud. We compared both version 7 and 8 AI for the scene on 4 August and find that those pixels that had values of 12.8 in version 7 are equal to or greater than roughly 18 in version 8. There are many such pixels in the scene on 4 August; the maximum is 28.9.

[16] Figures 8 and 9 show the AI (measured at approximately 1700 UTC) on 3 and 4 August, respectively. The 3 August TOMS view (Figure 8) is about 5 hours before convection began in earnest. Here the smoke is obviously abundant; the maximum AI = 12.2. The 4 August AI scenes in Figures 9a and 9b show consecutive orbits, at 1623 and 1801 UTC. These are within 2 hours of the AVHRR view of the croissant cloud in Figure 7c. The area of enhanced AI is

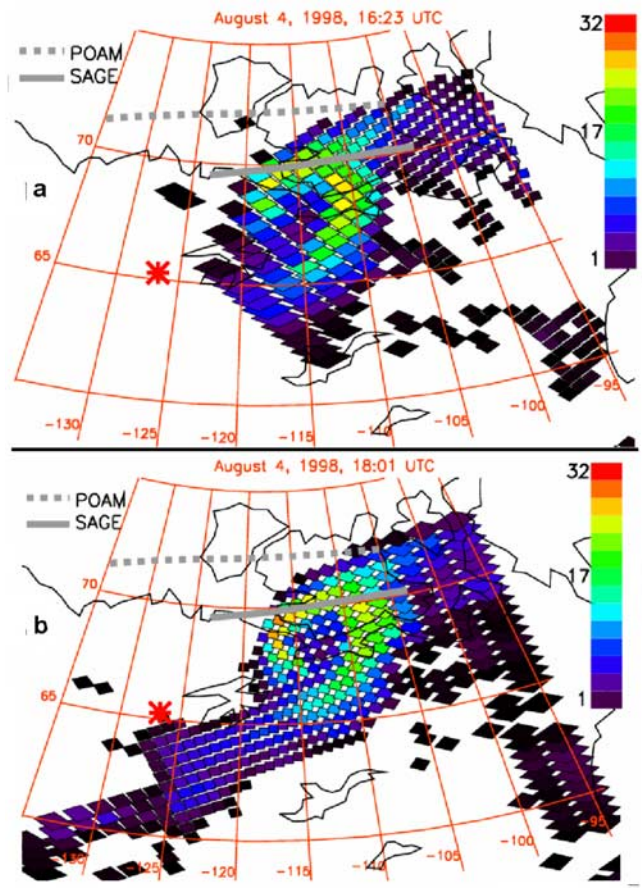

Figure 9. Same as Figure 8, but for two TOMS orbits on 4 August 1998. (a) 1623 UTC. (b) 1801 UTC. Gray lines are back trajectory segments for POAM (dashed line) and SAGE (solid line) aerosol layers presented in section displayed in Figure 14. Each segment spans the interval 0000 to 1800 UTC on 4 August.

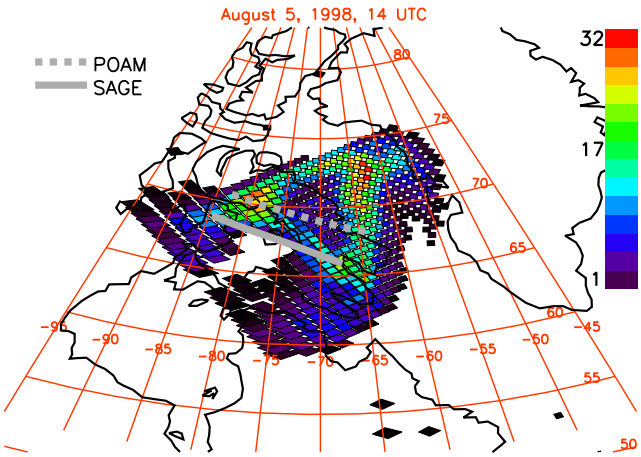

Figure 10. TOMS AI map for one orbit on 5 August 1998, 1400 UTC. Gray lines are back trajectory segments for POAM (dashed line) and SAGE (solid line) aerosol layers presented in Section displayed in Figure 14. Each segment spans the interval 0000 to 1400 UTC on 5 August.

even more widespread than on 3 August. The croissant cloud stands out, manifested by a nearly enclosed circle of particularly high AI (values greater than 18). Such a coherent area of extreme AI, coincident with gray visible and very cold IR imagery, has the same qualities as the Chisholm smoke plume described by FS03. Thus we can conclude that the croissant cloud is predominantly comprised of smoke aerosols.

[17] It is obvious from Figures 7c and 9a, which are only 5 min apart, that they signify a very unusual aerosol condition. We contend that the large values of AI identify extremes in aerosol plume altitude. The entire area of the croissant cloud, as manifested by the visible AVHRR image in Figure 7, is covered by extremely high AI values. Moreover, as discussed in relation to Figure 7c, a substantial part of the croissant plume is accompanied by very low IR T_b; hence the plume is at an unambiguously great altitude. The known strong dependence of TOMS AI on aerosol-layer altitude [*Hsu et al.*, 1999b] leads us to conclude that the entire croissant plume feature is in the UTLS, much deeper than the plume on 3 August. In addition to the plume altitude, the AI on these two consecutive orbits also confirms the rapid cyclonic circulation of the plume, and perhaps even rising in altitude. At 1623 UTC the maximum AI (values around 25) are in the northeast quadrant of the croissant cloud. By 1801 UTC the area of the peak AI has moved to the far western part of the evolving cyclone. Interestingly, it is at 1801 UTC that the greatest AI is recorded (28.9). At 1623 UTC the peak AI was situated over the coldest (thus unambiguously deep) part of the IR signature. By 1801 the peak-AI pixels were over an IR scene that was very warm (thus low or no cloud), but the peak AI increased at that time and place. AI is proportional to aerosol optical depth and plume altitude. We consider it unlikely (albeit possible) that the smoke cloud became more optically dense as it swirled and spread around the cyclone; thus we conclude that the peak altitude of the smoke plume may have actually increased in the 1623–1801 UTC interval. A full analysis of the relation between the AVHRR and AI data for this fascinating plume is called for, but is beyond the scope of this paper.

[18] The TOMS version 8 AI data provide strong evidence that the Norman Wells smoke plume in the lower stratosphere continued lofting to higher altitudes between 4 and 5 August. The peak AI on 5 August rose to 31.96 (Figure 10). On 5 August, there were 9 pixels, on two separate orbits (only one orbit is shown in Figure 10), with AI exceeding the peak 4 August value of 28.9. Considering that the plume had no additional source in the 4–5 August interval, and that it no doubt continued to disperse and incur

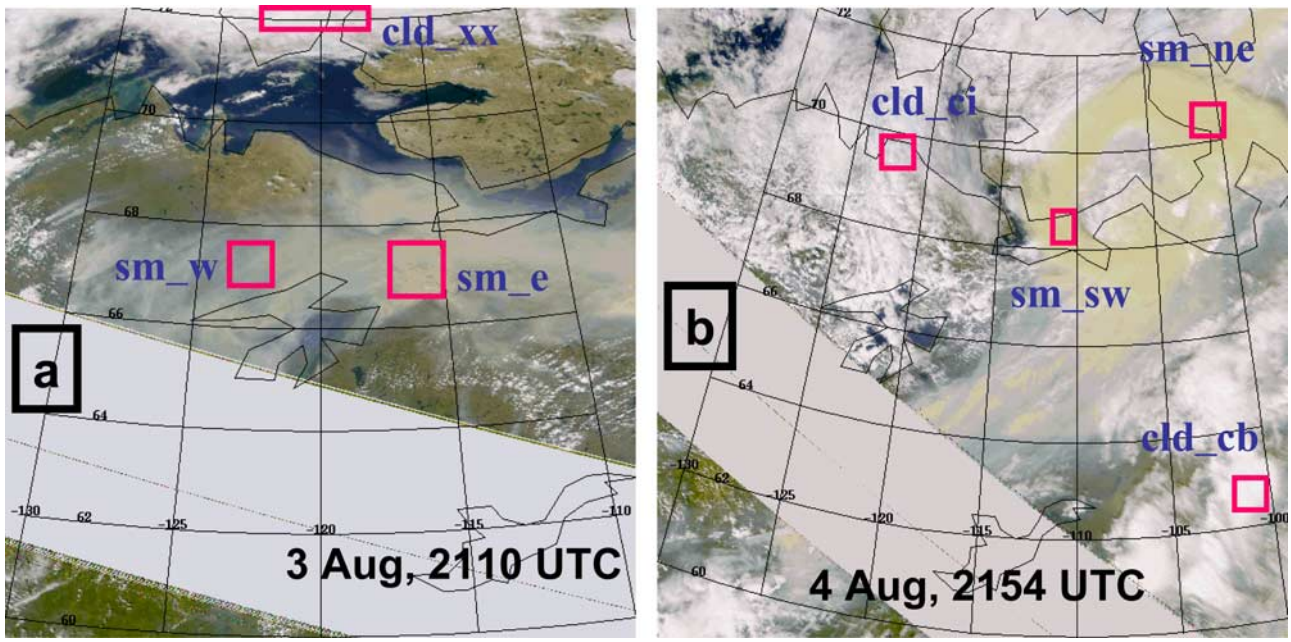

Figure 11. SeaWiFS true-color imagery, northwestern Canada for (left) 3 August 1998, 2110 UTC and (right) 4 August 1998, 2154 UTC. Gray swath is a no-data area. Each panel has colored rectangles showing cloud and smoke subscenes described in detail in the text and Table 1.

Table 1. Seven SeaWiFS Subscenes for Norman Wells PyroCb Smoke Color/Texture Analysis[a]

Scene	Mnemonic	Date	*n*
Cloud, undetermined	cld_xx	3 August	1020
Smoke east	sm_e	3 August	6528
Smoke west	sm_w	3 August	6318
Cirrus cloud	cld_ci	4 August	5820
Cumulonimbus anvil	cld_cb	4 August	368
Smoke northeast	sm_ne	4 August	1325
Smoke southwest	sm_sw	4 August	2600

[a]Refer to Figure 11 for mapped locations. Sample size is column *n*.

settling, we consider it unlikely that the peak optical depth of the plume would increase in two separate areas. Thus the only conclusion we can draw is that the topmost levels of the plume in the LS continued to be lofted, more than 36 hours after initial injection. *Pueschel et al.* [2000] put forward an argument for self-lofting of UTLS-level soot aerosols. Perhaps their mechanism, called gravito-photophoresis (sunlight-induced upward forcing), was at work in this case. This deserves continued study.

2.2.2. Unique Plume Color and Texture

[19] We now explore the color and texture of the smoke to learn more about the distinctiveness and evolution of the smoke from before the convection (3 August) to post-convection (4 August). Here we use the Sea-viewing Wide Field-of-view Sensor (SeaWiFS) true color imagery (Figure 11) [*Falke et al.*, 2001]. On 3 August the smoke being produced by the fires in this part of Canada was already intense and widespread, as shown by the SeaWiFS view at 2110 UTC (Figure 11a) and the AI in Figure 8. Figure 11b is the SeaWiFS view on 4 August at 2154 UTC. This is roughly 5 hours after the TOMS view, and clearly shows a continuing evolution of the plume shape. It appears that the deep smoke started in the early morning hours of 4 August as an elongated broad band, and then manifested a cyclonic circulation that resulted in the closed circular plume later in the day.

[20] Figure 11 has annotations marking features picked for the color/texture analysis. We identified rectangular areas in both images to capture cloud and smoke plume subscenes. The size of the rectangle (manually chosen) was picked to be small enough to guarantee homogeneity, but large enough to contain pixel counts sufficient for robust statistical analysis.

[21] Table 1 lists the subscenes by name, mnemonic, and sample size of SeaWiFS pixels contained therein. On 3 August, we picked an undetermined water-ice cloud-type scene ("cld_xx") and two portions of the broad smoke plume north of Great Bear Lake. The western portion ("sm_w") appears from Figure 11 to be less dense as compared to the richer brown segment to the east ("sm_e"). On 4 August we identified cirrus ("cld_ci") and deep convection ("cld_cb"), as well as portions of the most intense circular smoke plume ("smoke_sw" and "smoke_ne") that were very different in IR signature.

[22] Figure 12a contains the color analysis of these seven subscenes. Here we plot the average of the SeaWiFS radiance counts at three wavelengths (those used for the true-color imagery): blue (412 nm), green (555 nm), and red (670 nm). Brightness is proportional to radiance counts; whiteness comes from a balance of the three wavelengths, and brownness comes from a balance between, and dominance of, green plus red. As expected, the three cloud scenes on both days are quite similar in their whiteness. The brightness of the two 4 August clouds is greater than the cld_xx scene on 3 August, but all cloud scenes are brighter than the smoke scenes. Also as expected, the smoke color is distinct from the clouds; the blue component is small relative to red plus green. Comparing the smoke scenes before and after convection, though, reveals that the brownness actually becomes purer on 4 August; the blue component drops and red-plus-green increases.

[23] In section 2.2 the AVHRR visible imagery was used to point out the apparently extreme smoothness of the croissant plume. Here we use SeaWiFS to verify and analyze the smoke texture. Figure 12b is the texture analysis of the seven subscenes previously presented. The measure of scene smoothness is the standard deviation of the spectral radiance counts. Low standard deviation signifies a smooth surface; a greater standard deviation indicates more texture or inhomogeneity. The three cloud scenes are much alike, with roughly equal dispersion of counts in the blue, green, and red wavelengths. The smoke scenes are characterized by a dispersion in the blue that is about the same as or greater

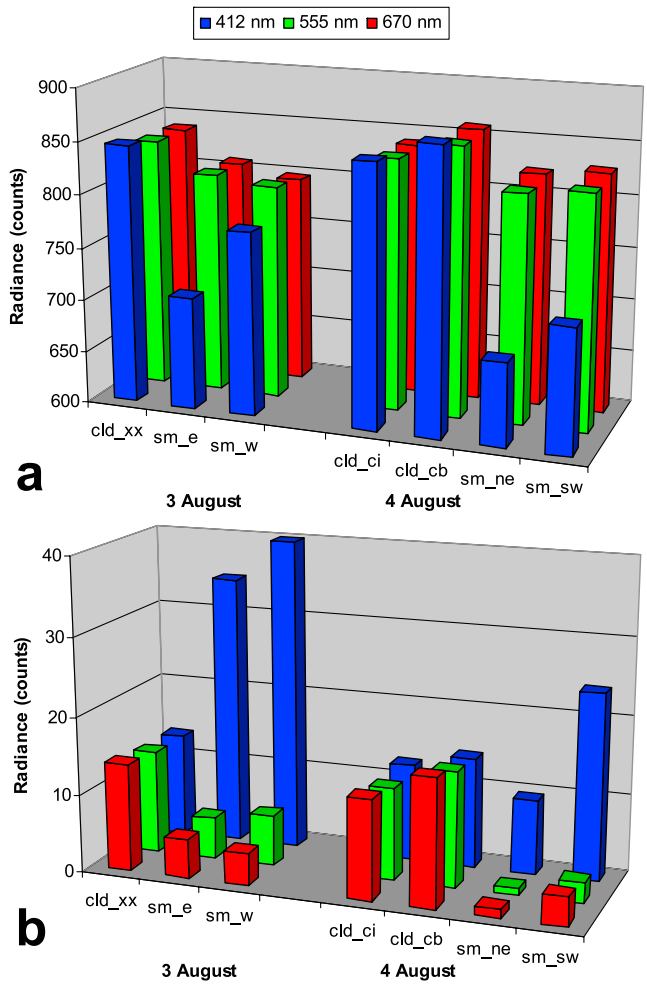

Figure 12. SeaWiFS radiance data (counts) at the true-color wavelengths used in Figure 11 (412, 555, and 670 nm) for the seven cloud and smoke subscenes identified in Table 1. (a) Average radiance. (b) Standard deviation.

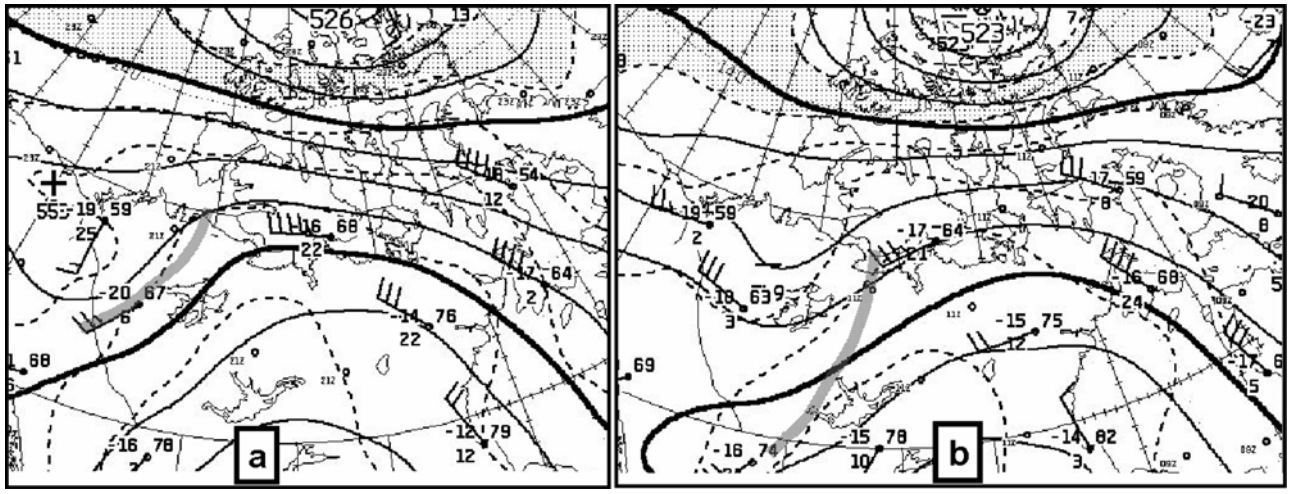

Figure 13. Upper air charts (500 hPa) for 4 August 1998, northwestern Canada. (a) 0000 UTC. (b) 1200 UTC. Height contours are solid, and contour interval is 60 m. Dashed contours are 1000–500 hPa thickness (proportional to mean column temperature). Also shown are radiosonde-station reports, using standard World Meteorological Organization layout and symbols. Gray arcing line is our analysis of the surface cold front at these two times.

than the water ice clouds, but with very little variability in the brighter red and green wavelengths (see Figure 12a). Thus it seems from the texture analysis of Figure 12b that the smoke scenes are characteristically smooth, relative to these three very different types of water-ice clouds. Moreover, the smoke plume on 4 August is even smoother than the smoke on 3 August, especially in the sm_ne scene. The standard deviation here is roughly one count out of an average of about 800 counts: extremely smooth. Such a lack of texture is consistent with the peculiarly stable state of the LS; thus this distinction itself might be highly suggestive of a stratospheric residence altitude.

[24] The northeast sector of the croissant cloud has the lowest IR T_b. Thus even though the sm_sw cloud is apparently at an extremely high altitude (according to the previous analysis of TOMS AI), the sm_ne cloud is unequivocally high and optically opaque, yet as ''smokey'' as any part of the smoke plume before or after convection. This is important to consider, in light of the fact that the UTLS-level smoke on 4 August was transported through water ice clouds and is apparently (according to the SeaWiFS true-color Figure 11 and the AVHRR views of Figure 7) intermingled with a variety of clouds. Thus the smoke in the croissant plume is effectively opaque in the visible spectrum, even in the coldest segment of the croissant cloud. This would indicate that the smoke in the sm_ne scene is perhaps an optically thick layer above a UTLS-level, dense water-ice cloud. It appears that the Norman Wells pyroCb produced and transported an enormous quantity of smoke, sufficient to create a UTLS-level pall that was broad in horizontal extent and at the same time nearly indistinguishable in content from the unambiguously great concentration of smoke before the blowup.

2.3. Meteorological Analysis

[25] Prior studies of extreme forest fire blowups have made a common association with synoptic scale meteorological conditions. *Fromm et al.* [2000] and FS03 reported that a pyroCb blowup with subsequent LS smoke transport occurred as a persistent anticyclone was replaced with a cold front moving through the blowup area. *Westphal and Toon* [1991] and *Murphy and Tymstra* [1986] found this meteorological association studying two earlier Canadian smoke palls, in July 1982 and September 1950, respectively. Those investigators did not raise the possibility of TST and likely did not suspect it either. However, the 4 August 1998 Norman Wells pyroCb event occurred under quite similar conditions. Figure 13 shows the operational 500-hPa weather analyses from the Canadian Meteorological Centre, at 0000 and 1200 UTC, 4 August, in northwestern Canada. A strong ridge is in place; the ridge line oriented approximately north-south through the landmass comprising NWT and Nunavut, roughly 110°W longitude. The surface cold front (our analysis, based on 1000 hPa height and wind-direction shift) connects with a low-pressure cell north of the NWT landmass and arcs south through the blowup area. On 4 August at 1200 UTC the 500-hPa ridge (Figure 13b) translated east roughly 10° in longitude, and a shortwave trough that was also evident at 0000 UTC (Figure 13a) has deepened and moved over the convective outbreak area. Hourly surface barometric pressure observations at Norman Wells (not shown) reveal that the advancing cold front passed though at approximately 0000 UTC on 4 August. Surface wind direction shifted and speed jumped by roughly a factor of 4 after frontal passage, to 8 m s^{-1}. (http://www.climate.weatheroffice.ec.gc.ca/climateData/canada_e.html). Daily high temperatures in Norman Wells on 1–3 August were 26.0°, 30.9°, and 27.9°C, respectively. The daily highs on 4–6 August were 22.5°, 20.7°, and 22.2°C, respectively. Thus a significant air mass change occurred, accompanied by 500-hPa-height falls, frontal uplift, and strong low-level wind in the vicinity of the cold front. The prior warm conditions and subsequent forcing no doubt played a role in creating and/or exacerbating the fire blowup potential by drying the fuel in advance of the destabilizing frontal uplift, which then generated or aided the numerous convective cells on or about 4 August.

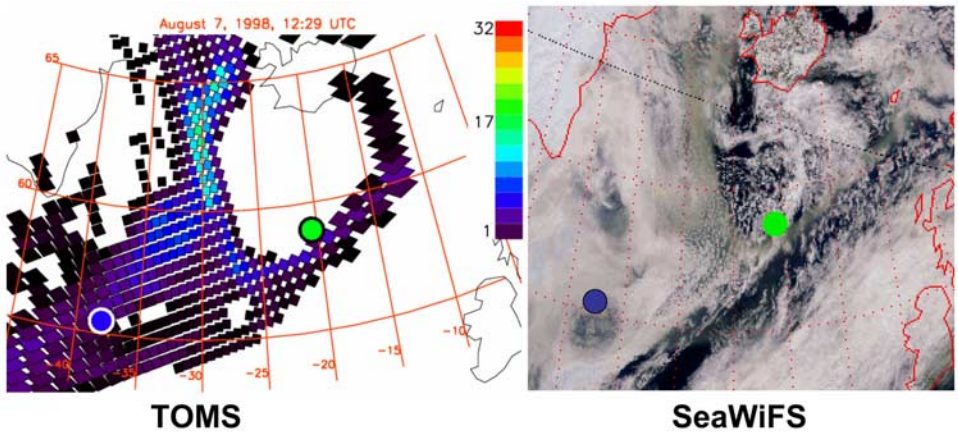

Figure 14. SeaWiFS true-color image and TOMS AI map, 7 August 1998, North Atlantic Ocean between southeastern Greenland and United Kingdom. Same AI color scale as for Figures 8–10 is used. Time of SeaWiFS is 1415 UTC; TOMS is 1229 UTC.

[26] In the context of the upper air charts just presented, the apparently cyclonic circulation of the Norman Wells smoke plume on 4 August is an intriguing aspect of this event. We have established that the smoke plume spread deeply through the troposphere and into the LS. Thus the circulation made evident by the smoke "tracer" appears to have been a feature that protruded deeply into the lower LS. The cyclonic swirl of smoke persisted well into 5 August, as seen in the AI (Figure 10). The occurrence of this circulation raises questions as to what caused it, whether the feature can be replicated with the available wind analyses, what role the intense heating of the many fires may have played, and what if any role the smoke itself played in the formation of this seemingly unusual condition. These would be worthwhile topics for future investigation but are beyond the scope of the present work.

2.4. Plume Altitude Observations

[27] On 7 August, 3 days after the Norman Wells blowup, a portion of the advected smoke plume was viewed by SeaWiFS and TOMS between Greenland and the United Kingdom (Figure 14). On this date the plume had spread across eastern North America, the Atlantic Ocean, and Greenland [*Hsu et al.*, 1999a]. Filmy brown smoke is readily apparent in the SeaWiFS image as a hazy area south of Greenland, a tongue running between Greenland and Iceland, and finer filament curling northeastward between Iceland and the United Kingdom. TOMS AI is in strong agreement here, and shows that the maximum AI is located in the tongue of aerosol between Greenland and Iceland. Once again, these two instruments together reveal, as they did on 4 August, a consistent feature: widespread, intense smoke aerosols. Figure 14 also shows that POAM III [*Lucke et al.*, 1999] and SAGE II [*Mauldin et al.*, 1985] sampled through different portions of this impressive plume on 7 August.

[28] The earliest evidence that allows us to precisely constrain the extent of TST by the Norman Wells pyroCb is given by these two POAM and SAGE profiles of aerosol extinction ratio (Figure 15). SAGE, at 38°W and POAM at 21°W observed unusual enhancements in the lower stratosphere. (Another POAM measurement in Figure 15, at 46°W, shows an unperturbed extinction profile.) The SAGE profile shows a strong aerosol enhancement at 12 km, 3 km above the tropopause. The tropopause height collocated with the SAGE and POAM data come from the dynamical definition, using potential vorticity (pv) and using the height at which pv = 3 pv units. PV is calculated from MET Office wind and temperature analyses [*Swinbank and O'Neill*, 1994]. The peak SAGE extinction (2.3×10^{-2} km^{-1}) is essentially the instrument's maximum measurable value [*Wang et al.*, 1995], here nearly a factor of 100 over Rayleigh extinction. The POAM measurement also indicates an aerosol enhancement, but does not resolve the profile below 13 km. The termination of the POAM profile

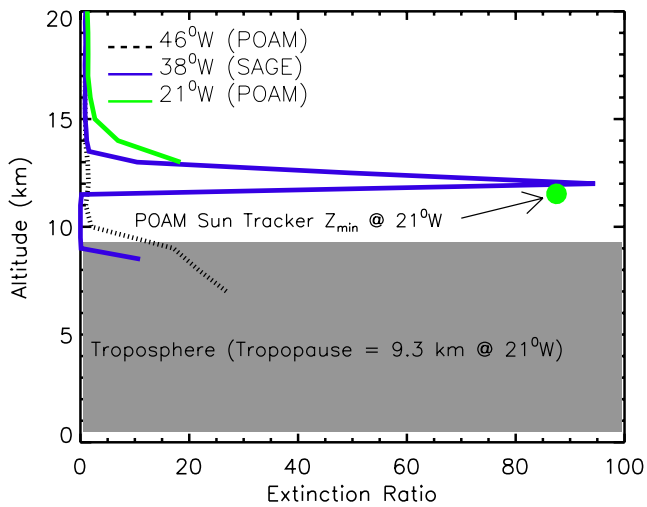

Figure 15. SAGE II and POAM III 1-μm extinction ratio (extinction/Rayleigh) profiles, 7 August 1998, over North Atlantic Ocean. Tropospheric altitudes are shaded gray. POAM measurement latitude is 58°N; SAGE is 55°N. Green dot shows altitude of termination of sun tracking for POAM measurement at 339°E. POAM profile at 314°E is typical of background conditions. The tropopause, defined by the height at which pv = 3 PVU, applies to the POAM location.

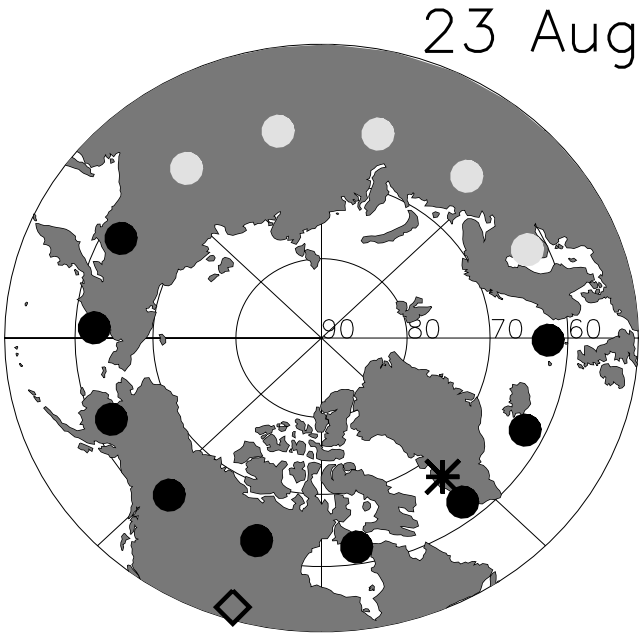

Figure 16. Location of lower stratospheric aerosol layers (black dots, asterisk, and diamond) on 23 August 1998. Diamond is location of backscatter/ECCsonde measurement. Asterisk is aerosol lidar location. Black dots are POAM locations. Light shading signifies no aerosol layer.

at this unusually high altitude is what *Fromm et al.* [1999] call a "High Zmin": Sufficiently optically thick clouds obscure the sun from the POAM sun tracker and cause it to terminate its measurements above the densest portion of the cloud. The POAM sun tracker Zmin is at approximately the altitude where SAGE detects the peak extinction of this extremely dense cloud (see Figure 15). The POAM measurement of enhanced extinction up to 15 km shows that the aerosol layer that peaks at 12 km extends to 6 km above the local tropopause. Although not shown, we have examined AVHRR visible and IR imagery at this time and determined that there were no high cirrus clouds that could have prejudiced our interpretation. Isentropic back trajectories, launched from the POAM and SAGE layers (358 and 360 K, respectively), have a path and speed that matches with the smoke cloud of 4 and 5 August (see Figures 9 and 10). Thus we contend that some portions of the TST from the Norman Wells pyroCbs reached 6 km above the tropopause and deposited high smoke concentrations in the LS. This is consistent with our estimates of plume height on 4 August based on minimum IR T_b and radiosonde temperature.

3. Stratospheric Impact: Observations

[29] The stratospheric impact of the TST events in summer 1998 was recorded by lidar and backscattersonde, as well as by SAGE and POAM. On 23 August, stratospheric layers of aerosol were detected by three independent instruments. On this date, POAM made 14 profile measurements, nine of which contained unambiguous aerosol enhancements up to 6 km above the tropopause. The map in Figure 16 shows where these observations were made at the POAM measurement latitude of 62°N. The aerosol layers were observed over a roughly 200° longitudinal extent, on nine consecutive orbits, suggestive of an essentially continuous aerosol feature. Figure 16 also shows locations of two other aerosol-layer observations at latitudes well poleward and equatorward of POAM. Over Greenland (67°N) at Sondrestromfjord, aerosol lidar [*Thayer et al.*, 1997] recorded an enhancement (Figure 17) that has fine structure and three layers between 13 and 15 km. Operational radiosonde measurements (http://raob.fsl.noaa.gov/) at 0000 UTC, 24 August, from Aasiaat, Greenland, 154 km north of the lidar site give a tropopause height of 9.2 km, temperature minimum at 11.8 km. Thus all three aerosol layers are well into the LS. From the radiosonde data we calculate a potential temperature of the highest layer (roughly 14.8 km) of 408 K, clearly in the stratospheric overworld.

[30] Also on that date a balloon payload with backscattersonde [*Rosen and Kjome*, 1991] and electro-chemical cell ozone sensor was launched near Saskatoon, Saskatchewan, and measured both aerosol and ozone on ascent, from the lower troposphere up to about 17 km altitude (Figure 18). The useful aerosol retrieval tops out at 16 km, but ozone was successfully retrieved up to 17.8 km. The balloon instruments recorded a remarkable phenomenon: coincident lower stratospheric enhancements of both aerosol backscatter and ozone abundance. It has been shown in tropospheric biomass burning plumes that ozone production can be expected and is observed [e.g., *Pickering et al.*, 1996; *Andreae et al.*, 2001]. However, a 0.3 ppmv increase over ambient conditions, in a highly elevated plume, is remarkable indeed, perhaps unprecedented. *Jost et al.* [2004] mentioned measurements of ozone in a biomass-burning plume in the LS in July 2002 that contained enhanced aerosols, CO, and H_2O, but with no apparent ozone increase (although the abundance was far greater than tropospheric values).

[31] Here the tropopause was about 10 km (according to the collocated temperature profile); above that level there were four distinct aerosol backscatter ratio peaks, the most dominant one at about 13.2 km altitude, corresponding to a potential temperature of 382 K. There were two primary layers of increased ozone, one relatively narrow between

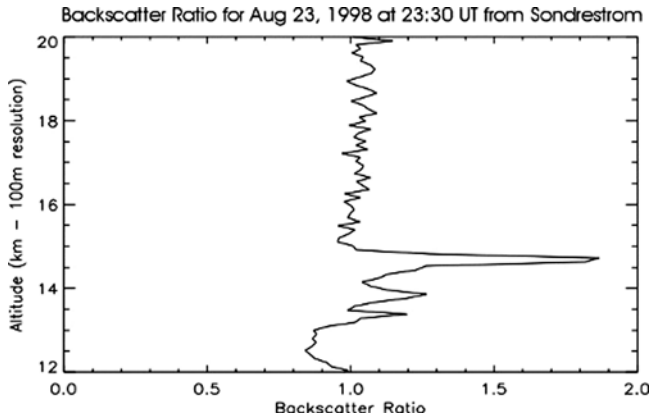

Figure 17. Lidar backscatter ratio profile on 23 August 1998 near Sondrestromfjord, Greenland (67°N, 51°W). The vertical resolution of the lidar is 100 m. The measurement wavelength is 532 nm. Note the three distinct aerosol layers between 13 and 15 km altitude.

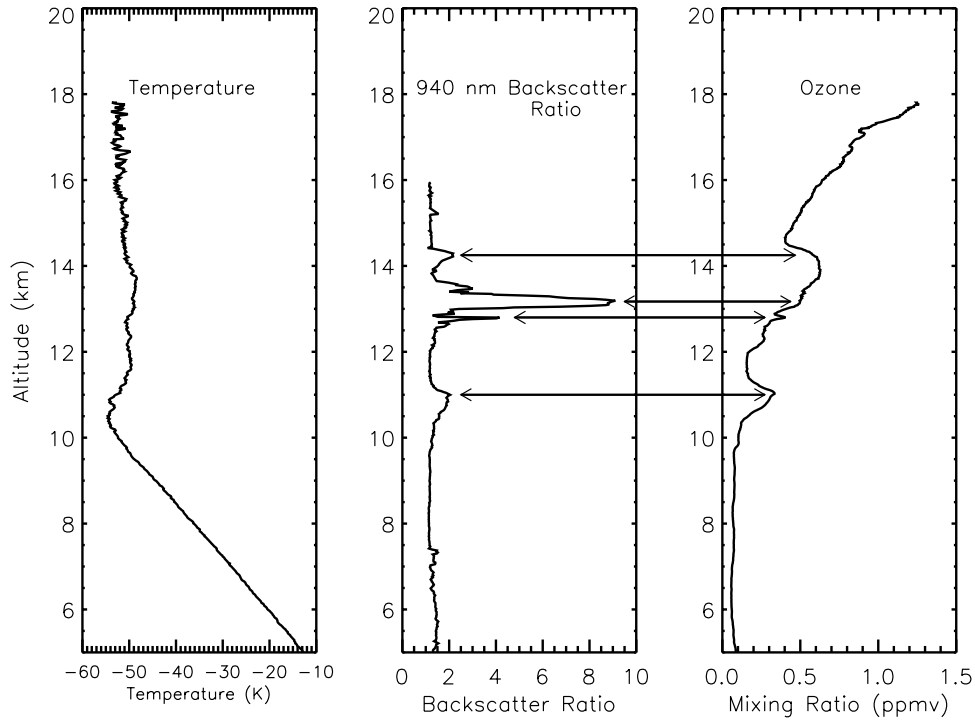

Figure 18. Sonde profiles, 23 August 1998, near Saskatoon, Canada (52°N, 107°W). (left) Temperature. (middle) Aerosol backscatter ratio at 940 nm. (right) Ozone mixing ratio.

about 10.5 and 11.3 km, and a stronger, broader layer from 12 km up to 14.5 km. In this layer, ozone peaked at roughly 0.6 ppmv, an approximate doubling of the expected background abundance at that altitude and even greater in relation to the tropospheric mixing ratios measured. There is a strong positive correlation even on a fine scale between the aerosol peaks and ozone. The arrows in Figure 18 point from the four most distinctive aerosol layer peaks to the corresponding part of the ozone profile. The three lowest aerosol layers all have coincident fine-scale ozone increases. We contend that these broad and fine-scale coincidences of increased aerosol backscatter ratio and ozone mixing ratio in Figure 18 suggest a common source for both constituents. In addition, we believe we can rule out two other possibilities, downward transport of both abundances and turbulent mixing. Downward transport, which would bring with it the higher ozone mixing ratios common at higher stratospheric levels, seems an unlikely explanation: There is no evidence in the POAM and SAGE data for the necessary aerosol abundance or recent formation from above. Turbulent mixing of increased ozone (and hence little aerosol) from above with smoke aerosols from the planetary boundary layer (thus with characteristically little ozone) would almost certainly produce poor or even negative correlation in the resultant mixture. It is beyond the scope of this paper to explore the mechanism for this unusually strong and perplexing ozone enhancement on 23 August 1998, but this revelation provides new insights into the impact of biomass burning on TST and chemistry. Such observations need to be explored more deeply in future measurement and modeling campaigns. Taken together, the 23 August POAM, lidar, and sonde measurements of aerosol and ozone enhancements signify an enduring perturbation resulting from extreme pyro-convection.

[32] Now we explore the evolution of the stratospheric part of the Norman Wells smoke plume. As reported by *Fromm et al.* [2000], POAM's daily zonal average lower stratospheric optical depth jumped by a factor of 5 in mid-August 1998. In Figure 19 the August daily median and maximum POAM 1018-nm extinction are displayed at several altitudes with respect to the tropopause height, from tropopause+1 km to tropopause+7 km. The daily sampling from which these values are calculated typically consists of 14 measurements at the POAM latitude (varying slowly from 58°N–65°N during August) each separated by about 25° in longitude. Each day's maximum extinction is only displayed in Figure 19 if that value exceeds 6 standard deviations (6σ) above an average computed from all of the POAM observations during the last 7 days of July. Thus the extremes shown represent only the severest departures from the norm. One other item displayed in Figure 19 is the daily occurrence of POAM High Zmin observations. Each day a count is made of profiles terminating with a sun tracker Zmin more than 3 km above the tropopause. Non-zero counts are shown in Figure 19. As mentioned previously, such High Zmins provide an additional, unique indication of stratospheric aerosol burden by identifying where particularly dense, "opaque" smoke cloud forms are occurring above the tropopause.

[33] We interpret Figure 19 as follows. The 6σ daily aerosol extrema were observed as far as 7 km above the tropopause after the Norman Wells blowup. However, the daily median was not tangibly altered at this altitude. From 1 to 6 km above the tropopause, there is a notable increase in the daily median extinction. In terms of average potential temperature of these tropopause-relative surfaces, the increase in daily median extends to approximately 430 K. The largest increase is at the tropopause+2 km (~380 K), where

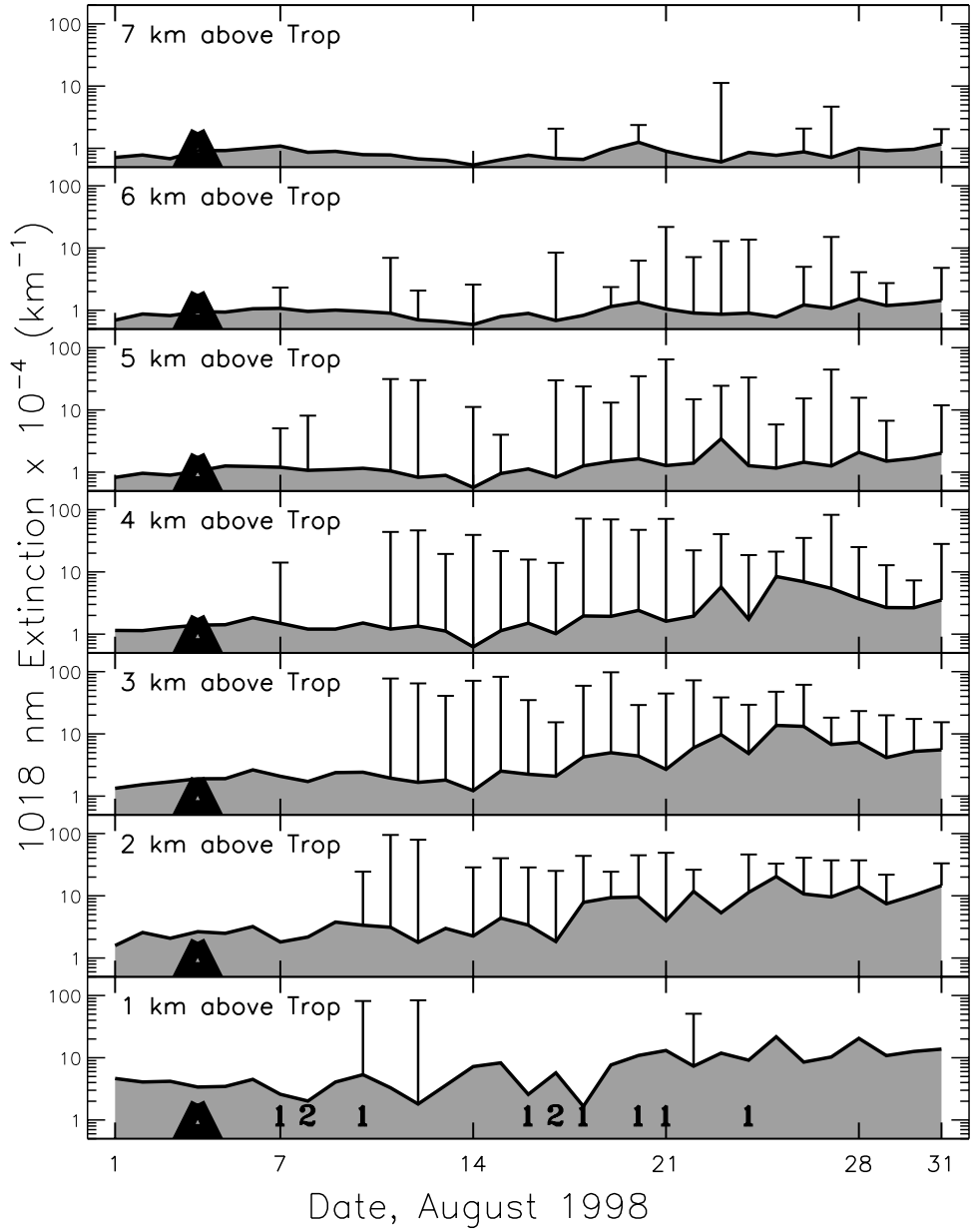

Figure 19. POAM III tropopause-relative 1018 nm extinction, 1 to 7 km above tropopause, August 1998. Daily median extinction is the solid line plot (with area below gray shaded for ease of viewing). Conical symbol at 4 August marks the date of the Norman Wells pyroCb blowup. Error-bar-type lines show the daily maximum extinction, for days on which the maximum was greater than 6 standard deviations from the pre-blowup daily average. Numerals along the abscissa show the count of POAM profiles on a given date that had a "high Zmin" profile termination.

the median in the last week of August was 5 times higher than during the first week. Since by its nature the median discounts the effect of outliers, this increase indicates a substantially perturbed aerosol burden in the LS. Although not shown, the daily occurrence frequency of POAM profiles with detectable stratospheric smoke layering increased through August. After 20 August, there were days when a majority of POAM profiles had a stratospheric aerosol layer (e.g., 23 August, illustrated by Figure 16). At altitudes 4 to 6 km above the tropopause, 6σ extrema appeared first on 7 August (e.g., the POAM profile in Figure 15). These extreme manifestations of aerosol increase became an essentially daily occurrence after 10 August between tropopause+1 km to tropopause+5 km. Hence we conclude that the smoke cloud was spreading and becoming a hemispheric phenomenon in August 1998.

[34] As impressive as these data are, it is still likely that the POAM data underestimate the true stratospheric aerosol increase. Along the timeline panel at tropopause+1, we indicate the daily count of POAM profiles with a High Zmin (as defined above). Forward modeling of the POAM sun tracker [*Fromm et al.*, 1999] indicates that the "center" altitude of the opaque cloud causing the High Zmin is roughly 1.25 km below the sun tracker Zmin. Hence such a

high termination indicates a large, albeit unmeasured, stratospheric aerosol layer peak on the order of 2 km above the tropopause. This is precisely what occurred on 7 August as seen in the SAGE and POAM profiles in Figure 15. Figure 19 shows that on 7, 8, and 10 August, four High Zmins were recorded. Although we do not show it, the location of the High Zmins on 8 and 10 August was very close to TOMS AI features, as was the case on 7 August.

[35] There was about a 1-week lull before another episodic increase in High Zmin frequency began. (There were no High Zmins in July or after August.) At this time (16–18 August) there were four more High Zmins. Three of the four were observed between 145°E and 155°E at 60°N. Isentropic back trajectories (launched on the 360 K potential temperature surface) from all four matched closely in space and time with forward trajectories launched from TOMS AI features on 13 August (over central Russia, 70°N, 81°E) that were traceable to the Norman Wells blowup. Even though the 16–18 August High Zmins were geographically close to smoke plumes coming off eastern Russian fires at that time [*Kasischke et al.*, 1999], the trajectories did not pass over the Russian combustion locale. Thus we conclude that this mid-month increase in opaque smoke-cloud sightings over eastern Russia and near the date line was also caused by the Norman Wells blowup. The presence of such optically thick LS smoke clouds 2 weeks after the TST episode is further testimony to the enormous atmospheric impact linked to this pyroCb. It is our finding that the Norman Wells pyroCb event on 4 August triggered a stratospheric intrusion of smoke, the detection of which was confirmed with POAM and SAGE aerosol profiles beginning about 7 August, an intrusion that increased the aerosol loading up to 7 km above the tropopause and spread over a hemispheric breadth. The aforementioned Russian fires of 1998 also produced persistent aerosol enhancements and also bursts of trans-Pacific transport; we continue to investigate these for evidence of other TST events in 1998.

4. Summary and Conclusions

[36] We have reported observations of a pyro-cumulonimbus event that occurred in the boreal forest of Northwest Territories Canada, near the town of Norman Wells, on 3–4 August 1998. This extreme blowup led to noteworthy tropospheric and stratospheric impact that has previously been reported in the literature. This report provides the first detailed assessment of the meteorological conditions during the "eruption," the explosive convection itself, and the specific "smoking gun" pyroCbs. In addition, we showed what we believe to be a first-ever observation of strongly enhanced ozone in the lower stratosphere in concert with the smoke layers. It is apparent from the satellite observations that between two and four extreme thunderstorm cells created a smoke pall of hemispheric scope that substantially increased stratospheric optical depth, injected aerosols up to 7 km above the tropopause (above ~430 K potential temperature), and also perturbed lower stratospheric ozone.

[37] The Norman Wells pyroCbs occurred during a summer (1998) of multiple pyroCb events, and was probably the single dominant TST event of that remarkable season. The meteorological setup and triggering conditions included a stagnant anticyclone that was followed by a cold frontal passage through a region of the boreal forest dotted with several persistent fires. This meteorological association with extreme forest fire blowups and subsequent long-range transport is consistent with other similar events reported in the literature [*Fromm and Servranckx*, 2003; *Fromm et al.*, 2000; *Livesey et al.*, 2004; *Westphal and Toon*, 1991; *Penndorf*, 1953]. The Norman Wells pyroCb event created an optically opaque, UTLS smoke cloud on the day after the blowup that was large in horizontal extent and unique in several respects. For instance, visible imagery showed this plume to be significantly less reflective (i.e., "browner") than water-ice clouds and also nearly absent of texture (i.e., smooth). Analysis of IR imagery and TOMS aerosol index showed unambiguously that the smoke residence altitude topped out in the UTLS. This plume also exhibited a curious cyclonic mesoscale circulation that was not evident in upper-air analyses. We used GOES IR imagery to trace the origin of this opaque, deep, large smoke plume back to the eruption of two to four thunderstorm cells in the vicinity of Norman Wells in the evening of 3 August 1998. This part of NWT was the scene of multiple fires and other convective cells, some associated with fires and others not. It appears that the pyro-convection was more extreme in vertical extent than the non-pyro-convection.

[38] We used POAM III and SAGE II profiles of aerosol extinction 3 days downstream to partially constrain the vertical extent of the Norman Wells pyroCb plume. Along with TOMS aerosol index and SeaWiFS true-color imagery, the SAGE and POAM data on 7 August showed that the smoke plume over the North Atlantic was resident as high as 6 km above the tropopause, still visible in the nadir, and opaque in POAM's field of view well above the tropopause. Later in August the frequency and intensity of stratospheric aerosol enhancements increased. By mid-month the zonal median POAM extinction, 2 km above the tropopause, increased five-fold over early August values. Aerosol enhancements were detectable up to 7 km above the tropopause. Considering the numerous enhancements observed by POAM, lidar, and backscattersonde, measuring on 23 August at a latitude range on the order of 15°, we conclude that the Norman Wells pyroCb TST had a significant hemispheric impact on the lowermost stratosphere.

[39] It is becoming increasingly apparent that the phenomenon of extreme pyro-convection is remarkably efficient as a mechanism for TST. Hence it is also increasingly apparent that many yet unresolved issues regarding these events need to be better understood. For instance, it is still unknown how much particulate matter was deposited in the UTLS by the Norman Wells pyroCbs. It will be important to study this and other cases in more detail, matching observations with realistic cloud modeling of transport, microphysics, and chemistry to reconcile the observed smoke cloud and ozone enhancement signatures. It is also necessary to develop better estimates of boundary layer forcing, in terms of energy release rates, frontal lifting, and dynamical interaction between cloud, lightning, wind, fire activity, and combustion efficiency in order to arrive at aerosol (and other emission) production amounts. In short, the challenge will be to reconcile the observed aerosol burden from features such as the croissant cloud on 4 August 1998 with the fuel and area burned during the convective activity.

[40] Other issues in need of exploration include the occurrence frequency of the pyroCb phenomenon and the precise, combined factors that feed this important event. An aspect of this uncertainty that deserves scrutiny is the question of how efficient non-fire-related extreme convection is with regard to deep transport. Because *Wang* [2003] and others have observed and modeled plumes above such thunderstorms, it is reasonable to expect a new appreciation for the role of severe convection in transport of greenhouse gases and other boundary layer material to the UTLS.

[41] **Acknowledgments.** We thank Julie Dion for composing the AVHRR and GOES images. We are grateful to Tom Lee and Kim Richardson of NRL Monterey for help with visualizing DMSP OLS data. TOMS AI mapping codes were supplied by Gordon Labow of NASA GSFC. J. M. R. was supported by National Science Foundation (NSF) Grant ATM-0086484. J. P. T. was supported by the NSF Cooperative Agreement, ATM-0334122.

References

Andreae, M., et al. (2001), Transport of biomass burning smoke to the upper troposphere by deep convection in the equatorial region, *Geophys. Res. Lett.*, *28*, 951–954.

Andreae, M., D. Rosenfeld, P. Artaxa, A. Costa, G. Frank, K. Longo, and M. Silva Dias (2004), Smoking rain clouds over the Amazon, *Science*, *303*, 1337–1342.

Arking, A., and J. Childs (1985), The retrieval of cloud cover parameters from multispectral satellite images, *J. Clim. Appl. Meteorol.*, *24*, 322–333.

Falke, S., R. Husar, and B. Schichtel (2001), Fusion of SeaWiFS and TOMS satellite data with surface observations and topographic data during extreme aerosol events, *J. Air Waste Manage. Assoc.*, *51*, 1579–1585.

Fiebig, M., A. Petzold, U. Wandinger, M. Wendisch, C. Kiemle, A. Stifter, M. Ebert, T. Rother, and U. Leiterer (2002), Optical closure for an aerosol column: Method, accuracy, and inferable properties applied to a biomass-burning aerosol and it radiative forcing, *J. Geophys. Res.*, *107*(D21), 8130, doi:10.1029/2000JD000192.

Formenti, P., et al. (2002), STAAARTE-MED 1998 summer airborne measurements over the Aegean Sea: 1. Aerosol particles and trace gases, *J. Geophys. Res.*, *107*(D21), 4550, doi:10.1029/2001JD001337.

Forster, C., et al. (2001), Transport of boreal forest fire emissions from Canada to Europe, *J. Geophys. Res.*, *106*, 22,887–22,906.

Fromm, M., and R. Servranckx (2003), Transport of forest fire smoke above the tropopause by supercell convection, *Geophys. Res. Lett.*, *30*(10), 1542, doi:10.1029/2002GL016820.

Fromm, M., R. Bevilacqua, J. Hornstein, E. Shettle, K. Hoppel, and J. Lumpe (1999), An analysis of Polar Ozone and Aerosol Measurement (POAM) II Arctic polar stratospheric cloud observations, 1993–1996, *J. Geophys. Res.*, *104*, 24,341–24,357.

Fromm, M., J. Alfred, K. Hoppel, J. Hornstein, R. Bevilacqua, E. Shettle, R. Servranckx, Z. Li, and B. Stocks (2000), Observations of boreal forest fire smoke in the stratosphere by POAM III, SAGE II, and lidar in 1998, *Geophys. Res. Lett.*, *27*, 1407–1410.

Holton, J. R., P. H. Haynes, E. M. McIntyre, A. R. Douglass, R. B. Rood, and L. Pfister (1995), Stratosphere-troposphere exchange, *Rev. Geophys.*, *33*, 403–439.

Hsu, N. C., J. Herman, J. Gleason, O. Torres, and C. Seftor (1999a), Satellite detection of smoke aerosols over a snow/ice surface by TOMS, *Geophys. Res. Lett.*, *26*, 1165–1168.

Hsu, N., J. Herman, O. Torres, B. Holben, D. Tanre, T. Eck, A. Smirnov, B. Chatenet, and F. Lavenu (1999b), Comparisons of the TOMS aerosol index with Sun-photometer aerosol optical thickness: Results and applications, *J. Geophys. Res.*, *104*, 6269–6279.

Jost, H., et al. (2004), Observations of mid-latitude forest fire plumes deep in the stratosphere, *Geophys. Res. Lett.*, *31*, L11101, doi:10.1029/2003GL019253.

Kasischke, E., and J. Penner (2004), Improving global estimates of atmospheric emissions from biomass burning, *J. Geophys. Res.*, *109*, D14S01, doi:10.1029/2004JD004972.

Kasischke, E., K. Bergen, R. Fennimore, F. Sotelo, G. Stephens, A. Janetos, and H. Shugart (1999), Satellite imagery gives clear picture of Russia's boreal forest fires, *Eos Trans. AGU*, *80*, 143–147.

Lindesay, J., M. Andreae, J. Goldammer, G. Harris, H. Annegarn, M. Garstang, R. Scholes, and B. Wilgen (1996), International Geosphere-Biosphere Programme/International Global Atmospheric Chemistry SAFARI-92 field experiment: Background and overview, *J. Geophys. Res.*, *101*, 23,521–23,530.

Livesey, N., M. Fromm, J. Waters, G. Manney, M. Santee, and W. Read (2004), Enhancements in lower stratospheric CH_3CN observed by UARS MLS following boreal forest fires, *J. Geophys. Res.*, *109*, D06308, doi:10.1029/2003JD004055.

Lucke, R., et al. (1999), The Polar Ozone and Aerosol Measurement (POAM) III instrument and early validation results, *J. Geophys. Res.*, *104*, 18,785–18,799.

Mauldin, L., N. Zaun, M. McCormick, J. Guy, and W. Vaughn (1985), Stratospheric Aerosol and Gas Experiment II Instrument: A functional description, *Opt. Eng.*, *24*, 307–312.

Murphy, P., and C. Tymstra (1986), The 1950 Chinchaga River fire in the Peace River region of British Columbia/Alberta: Preliminary results of simulating forward spread distances, paper presented at Third Western Region Fire Weather Committee Scientific and Technical Seminar, Can. For. Serv., Edmonton, Alberta, Canada.

O'Neill, N., T. Eck, B. Holben, A. Smirnov, A. Royer, and Z. Li (2002), Optical properties of boreal forest fire smoke derived from Sun photometry, *J. Geophys. Res.*, *107*(D11), 4125, doi:10.1029/2001JD000877.

Penndorf, R. (1953), On the phenomenon of the colored sun, especially the "blue" sun of September 1950, *Tech. Rep. 53-7*, 41 pp., Air Force Cambridge Res. Cent., Cambridge, Mass.

Pickering, K., et al. (1996), Convective transport of biomass burning emissions over Brazil during TRACE-A, *J. Geophys. Res.*, *101*, 23,993–24,012.

Poulida, O., R. Dickerson, and A. Heymsfield (1996), Stratosphere-troposphere exchange in a midlatitude mesoscale convective complex: 1. Observations, *J. Geophys. Res.*, *101*, 6823–6836.

Pueschel, R., S. Verma, H. Rohatschek, G. Ferry, N. Boiadjieva, S. Howard, and A. Strawa (2000), Vertical transport of anthropogenic soot aerosol into the middle atmosphere, *J. Geophys. Res.*, *105*, 3727–3736.

Rosen, J. M., and N. T. Kjome (1991), Backscattersonde: A new instrument for atmospheric aerosol research, *Appl. Opt.*, *30*, 1552–1561.

Sherwood, S. C., J.-H. Chae, P. Minnis, and M. McGill (2004), Underestimation of deep convective cloud tops by thermal imagery, *Geophys. Res. Lett.*, *31*, L11102, doi:10.1029/2004GL019699.

Spichtinger, N., M. Wenig, P. James, T. Wagner, U. Platt, and A. Stohl (2001), Satellite detection of a continental-scale plume of nitrogen oxides from boreal forest fires, *Geophys. Res. Lett.*, *28*, 4579–4582.

Stohl, A., et al. (2003), Stratosphere-troposphere exchange: A review, and what we have learned from STACCATO, *J. Geophys. Res.*, *108*(D12), 8516, doi:10.1029/2002JD002490.

Swinbank, R., and A. O'Neill (1994), A stratosphere-troposphere data assimilation system, *Mon. Weather Rev.*, *122*, 686–702.

Thayer, J. P., N. B. Nielsen, R. Warren, C. J. Heinselman, and J. Sohn (1997), Rayleigh lidar system for middle atmosphere research in the arctic, *Opt. Eng.*, *36*, 2045–2061.

Wallace, J. M., and P. V. Hobbs (1977), *Atmospheric Science: An Introductory Survey*, 467 pp., Elsevier, New York.

Wandinger, U., et al. (2002), Optical and microphysical characterization of biomass-burning and industrial-pollution aerosols from multiwavelength lidar and aircraft measurements, *J. Geophys. Res.*, *107*(D21), 8125, doi:10.1029/2000JD000202.

Wang, P. K. (2003), Moisture plumes above thunderstorm anvils and their contributions to cross-tropopause transport of water vapor in midlatitudes, *J. Geophys. Res.*, *108*(D6), 4194, doi:10.1029/2002JD002581.

Wang, P., M. McCormick, P. Minnis, G. Kent, G. Yue, and K. Skeens (1995), A method for estimating vertical distribution of the SAGE II opaque cloud frequency, *Geophys. Res. Lett.*, *22*, 243–246.

Westphal, D., and O. Toon (1991), Simulations of microphysical, radiative, and dynamical processes in a continental-scale forest fire smoke plume, *J. Geophys. Res.*, *96*, 22,379–22,400.

R. Bevilacqua, Naval Research Laboratory, Code, 7200, 4555 Overlook Avenue, SW, Washington, D. C. 20375, USA.

M. Fromm, Naval Research Laboratory, Code 7227, 4555 Overlook Avenue, SW, Washington, D. C. 20375, USA. (mike.fromm@nrl.navy.mil)

J. Herman, NASA Goddard Space Flight Center, Code 613.3, Greenbelt, MD 20771, USA.

D. Larko, Science Systems and Applications, Inc., Suite 500, 10210 Greenbelt Road, Lanham, MD 20706, USA.

J. Rosen, Department of Physics and Astronomy, University of Wyoming, Department 3905, Laramie, WY 82071, USA.

R. Servranckx, Canadian Meteorological Centre, 2121 North Service Road, Trans-Canada Highway, Dorval, Quebec, Canada H9P 1J3.

J. P. Thayer, Department of Aerospace Engineering Sciences, University of Colorado, Engineering Center, ECOT-612, Boulder, CO 80309-0429, USA.